Effect of the switching pattern of the illumination of dynamic apertures on the ranges of the generated localized waves

Amr M. Shaarawi and Sherif M. Sedky

Department of Engineering Physics and Mathematics, Faculty of Engineering, Cairo University, Giza, Egypt

Richard W. Ziolkowski

Electromagnetics Laboratory, Department of Electrical and Computer Engineering, University of Arizona, Tuscon, Arizona 85721

Fawzia M. M. Taiel

Department of Engineering Physics and Mathematics, Faculty of Engineering, Cairo University, Giza, Egypt

Received July 3, 1995; accepted February 23, 1996

We study two different switching patterns of dynamic apertures illuminated by a focus-wave-mode excitation field. The two sources are chosen to be identical except that one is illuminated with use of a Gaussian time window, whereas the other uses a periodic function defined over the same time span. In spite of the similarity between the two dynamic apertures, the decay patterns of the amplitudes of their radiated fields are significantly different. A detailed analysis of the depletion of their spectral contents shows that the coupling between the spatial and temporal spectral components plays a decisive role in extending the range of the localization of the radiated pulses. © 1996 Optical Society of America.

1. INTRODUCTION

In a study concerning the causality of the focus wave modes (FWM's),[1] it has been shown that a causal FWM pulse can be generated from a dynamic Gaussian aperture.[1–3] A source of this type is driven by a Gaussian illumination characterized by the time variation of its effective radius. If the excitation wave field is allowed to illuminate an aperture situated at $z = 0$ for an infinitely long period of time, the generated FWM pulse propagates without any dispersion into the $z > 0$ half-space.[1] Furthermore, it has been demonstrated that an approximation to the FWM field[4] can be generated from a dynamic Gaussian aperture illuminated by a time-limited excitation wave field.[2] In this case the generated pulse holds out as it propagates to a finite range beyond which it starts to decay. The performance of such an aperture has been studied in detail. Such a dynamic source provides an efficient scheme to launch narrow Gaussian pulses from extended apertures.[1–3]

The FWM belongs to a wider class of solutions that has come to be called localized waves.[4–15] Such pulsed fields exhibit extended ranges of localization and are characterized by their large bandwidths. The spatial and temporal frequency components of their excitation wave fields are strongly coupled together. A combination of the time-limited excitation of the FWM pulse and the temporal–spatial distribution of the various elements constituting its aperture can have a direct impact on its spreading as it propagates away from the source plane.[2,3,15] In this paper, we investigate the effects of time limiting the excitation of the aperture on the depletion of the spectral components of the generated wave field. The depletion of the spectral content of the propagating pulse shows exactly how its centroid holds out for a specific range and why it starts to spread out beyond a certain point.

In this paper the FWM wave field is used to illuminate a dynamic aperture situated at $z = 0$. However, such a field exists over an infinite time span. To time limit the excitation of the dynamic aperture, we use a window function to cut off the infinite FWM excitation. In particular, we use two time windows; the first is a Gaussian function, and the second is a periodic window restricted to the time span of the first window. Thus the main difference between the two excitation wave fields is that one is turned on and off several times over the same time period throughout which the other one is on. However, the two excitation fields are chosen to share the same spatial spectrum. Hence the two generated localized pulses have equal initial radii. Moreover, the ultrawide temporal bandwidths of the two pulses are indistinguishable because they differ only by the spectral widths of their switching windows, which are negligibly small in comparison with the total bandwidths. As the pulses propagate away from the source, the depletion of the spectral components in the two situations exhibits a low-pass-filtering effect, in which the contributions from the switching spectral windows centered around the lower spatial frequency components are removed first. Such a depletion causes the amplitude of the pulse traveling away from the aperture to decrease with distance. This

0740-3232/96/0801712-07$10.00

issue is investigated in detail because it illustrates exactly when and how the amplitude of the pulses starts to decay. It will be shown that even though the bandwidths of the two illumination fields are similar and the waists of the initial pulses are equal, the amplitude of the propagating field decays differently in the two situations.

2. INITIAL ILLUMINATION OF TWO FINITE DYNAMIC APERTURES

It has been established that finite-energy localized-wave solutions can be generated from dynamic apertures.[2,3] Such sources are characterized by ultrawide frequency bandwidths at the same time that they exhibit a strong correlation between their spatial and temporal frequency components. In a previous study[2] we demonstrated that a pulse that approximates the FWM can be generated from a dynamic aperture that shrinks from its maximum initial size at $t = -4T$ to its smallest radius at $t = 0$ and then expands back to its original size at $t = 4T$. In order to limit the extension of the initial excitation of a dynamic aperture, we use a time window. In this section we investigate the illumination of two apertures excited by the same initial field but controlled by two different time windows. The first has a Gaussian distribution of the form $\exp(-t^2/4T^2)$. This function will effectively force the initial excitation to exist over the time span given by $-4T \leqslant t \leqslant 4T$. The second time window has a periodic distribution, which is explicitly defined as $\cos^2(5\pi t/8T)$ for $-4T \leqslant t \leqslant 4T$. Figure 1 displays the two windows under consideration. From the figure it is clear that the periodic time window is turned on and off several times over the same time span that the Gaussian window is on.

Throughout this paper we shall refer to the aperture controlled by the Gaussian time window as a Gaussian aperture, and that controlled by the periodic window as a periodic aperture. In both cases the initial field exciting the aperture is considered to have the same spectrum as

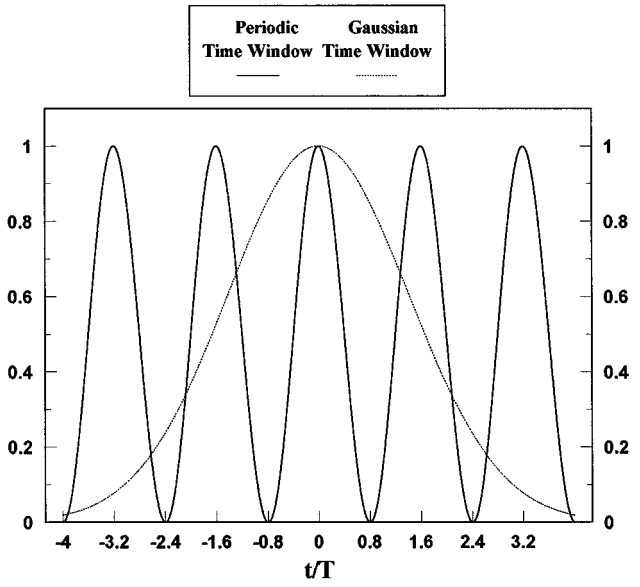

Fig. 1. Time windows of the excitation of the periodic and the Gaussian apertures.

that of the FWM source-free solution[14,16] after the corresponding time window has been applied. In particular, the initial field exciting the Gaussian aperture is assumed to have the following form:

$$\Psi(\rho, t) = \mathrm{Re}\{\hat{\Psi}(\rho, t)\},$$

where

$$\hat{\Psi}(\rho, t) = \frac{1}{4\pi(a_1 - ict)} \exp[-\beta\rho^2/(a_1 - ict)] \times \exp(i\beta ct)\exp(-t^2/4T^2), \tag{2.1}$$

whereas for the periodic aperture the initial field is

$$\hat{\Psi}(\rho, t) = \frac{1}{4\pi(a_1 - ict)} \exp[-\beta\rho^2/(a_1 - ict)] \times \exp(i\beta ct)\cos^2(5\pi t/8T), \tag{2.2}$$

for $-4T < t < 4T$ and is equal to zero otherwise. From Eqs. (2.1) and (2.2) we can see that the illumination fields driving the two apertures have the same effective time-dependent radius $\sim O(ct/\sqrt{\beta a_1})$. Thus the two sources are effectively varying their sizes with time. Since the two apertures are illuminated for the same time interval, their maximum radii are equal.

It has been shown in previous work[1] that the source-free FWM field can be represented as a superposition of forward- and backward-propagating components.[17] To produce a FWM pulse dominated by the forward-propagating field components, we must choose $\beta a_1 \ll 1$.[3] The same condition is needed here in order to launch causal approximations of the FWM pulse efficiently from a dynamic aperture. A reasonable selection is to take $\beta = 1.25\ \mathrm{m}^{-1}$ and $a_1 = 0.00001$ m. The period of illumination of the aperture is chosen to be $cT = 6.25$ mm, where c is the speed of light.

The Fourier spectrum of the initial excitation has a direct effect on the behavior of the pulse as it propagates away from the aperture. Hence it is convenient to start by studying the Fourier spectral content in each case. We define the Fourier spectrum as

$$\phi(\chi,\omega) = \int_{-\infty}^{\infty} dt \int_0^{\infty} d\rho J_0(\chi\rho)\rho \exp(-i\omega t)\hat{\Psi}(\rho, t). \tag{2.3}$$

The Fourier spectrum of the initial excitation of the Gaussian aperture can be obtained by substituting Eq. (2.1) into Eq. (2.3) and integrating over ρ and t, yielding

$$\phi(\chi, \omega) = \frac{1}{4\beta} \hat{\delta}_G[\omega - \omega_0(\chi); cT]\exp(-\chi^2 a_1/4\beta),$$

where

$$\hat{\delta}_G[\omega - \omega_0(\chi); cT] = \frac{T}{\sqrt{\pi}} \exp\{-T^2[\omega - \omega_0(\chi)]^2\} \tag{2.4}$$

is the Gaussian $\hat{\delta}_G$ function, whose width depends on T, and its central value $\omega_0 = (\chi^2/4\beta + \beta)c$ is a function of the χ variable.

The initial illumination of the periodic aperture has a Fourier spectrum obtained by substituting Eq. (2.2) into Eq. (2.3) and integrating over ρ and t to obtain

$$\phi(\chi,\omega) = \frac{1}{4\beta}\,\hat{\delta}_P[\omega - \omega_0(\chi);\, cT]\exp(-\chi^2 a_1/4\beta),$$

where

$$\hat{\delta}_P[\omega - \omega_0(\chi);\, cT] = \frac{1}{2\pi}\sin\{[\omega - \omega_0(\chi)]4T\}\left(\frac{1}{[\omega - \omega_0(\chi)]} - \frac{[\omega - \omega_0(\chi)]}{\{[\omega - \omega_0(\chi)]^2 - (5\pi/4T)^2\}}\right) \tag{2.5}$$

is the periodic $\hat{\delta}_P$ function. Figure 2 displays the spectra given in Eqs. (2.4) and (2.5) at $\chi = 0$. From the figure it is clear that the Fourier spectrum of the periodic aperture has an ω window that is larger than that of the Gaussian aperture even though its central lobe is narrower. Furthermore, the periodic spectrum is characterized by having negative and positive spectral amplitudes, whereas the Gaussian spectrum does not have any negative components.

We notice that in the limit as $T \to \infty$, the Gaussian $\hat{\delta}_G$ function and the periodic $\hat{\delta}_P$ function in Eqs. (2.4) and (2.5) reduce to the Dirac δ function. The latter characterizes the spectra corresponding to infinite-time excitations of dynamic apertures.[1] For the large values of cT, the Gaussian and periodic spectral functions reduce to a narrow distribution with a small bandwidth $\delta\omega \sim O(2\pi/T)$, for which $\omega \sim \omega_0(\chi) = [(\chi^2/4\beta) + \beta]c$. Such a narrow frequency window varies with χ and provides most of the significant contributions to the amplitude of the centroid of the pulse.

The initial illumination of the aperture utilizes a wideband field whose temporal and spatial frequency components are coupled together through the $\hat{\delta}$ functions given in Eqs. (2.4) and (2.5). Such a coupling does not exist for quasi-monochromatic continuous-wave excitations. In contradistinction to the continuous-wave radiation characterized by a single carrier frequency, the localized-wave pulses have ultrawide frequency bandwidths. Hence we have to set a criterion to specify the maximum frequency components for the temporal and spatial spectra. We choose to define the maximum spatial and temporal frequencies as those at which the amplitude of the spectrum drops to $(1/e^4)$ of its maximum value. In order to decouple the temporal from the spatial frequency components, we define the spatial spectrum as

$$\phi_s(\chi,\, t) = \frac{1}{2\pi}\int_0^\infty d\omega\,\phi(\chi,\omega)\exp(i\omega t). \tag{2.6}$$

The spatial spectrum of the Gaussian aperture is obtained by substituting Eq. (2.4) into Eq. (2.6) to produce

$$\phi_s(\chi,\, t) = \frac{\exp(-\chi^2 a_1/4\beta)}{8\pi\beta}\exp[-i\omega_0(\chi)t] \times \exp(-t^2/4T^2). \tag{2.7}$$

In Fig. 3 we display $\phi_s(\chi, 0)$ where it is clear that most of the significant components of the χ spectrum are concentrated at the lower end of the spectrum. High oscillations introduced into the ω windows sweeping the lower χ frequencies cause the pulse to decay as it propagates away from the aperture. The bandwidth of the χ spectrum, as is clear from the figure, is $\Delta\chi = 1415\ \mathrm{m}^{-1}$.

The periodic aperture has a spatial spectrum obtained by substituting Eq. (2.5) into Eq. (2.6), which explicitly gives

$$\phi_s(\chi,\, t) = \frac{\exp(-\chi^2 a_1/4\beta)}{8\pi\beta}\cos^2(5\pi t/8T) \times \exp[i\omega_0(\chi)t], \qquad -4T \leq t \leq 4T. \tag{2.8}$$

It is obvious that the two spatial spectra given in Eqs. (2.7) and (2.8) are identical when $t = 0$. In both cases

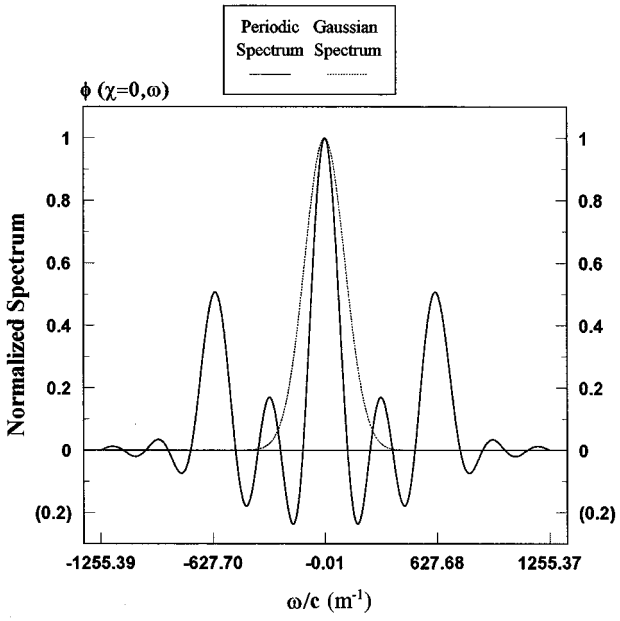

Fig. 2. Fourier spectra of the illuminations of the periodic and the Gaussian apertures.

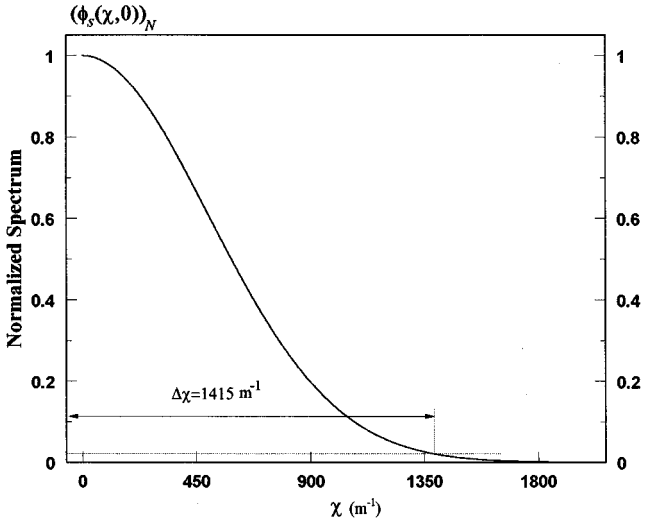

Fig. 3. Spatial spectrum of the illumination of the Gaussian aperture.

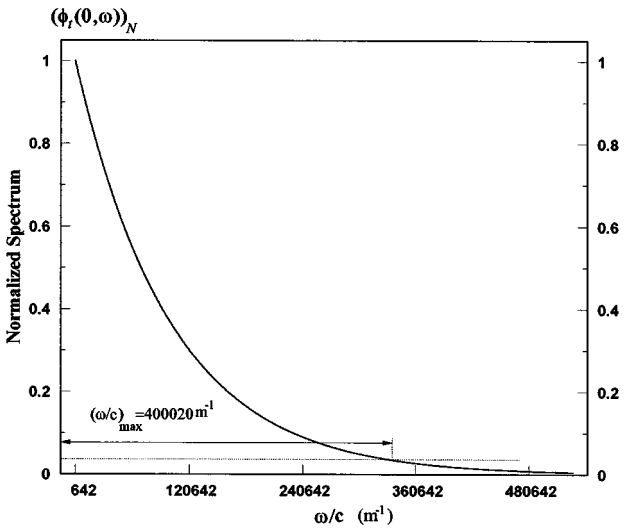

Fig. 4. Temporal spectrum of the illumination of the Gaussian aperture.

the bandwidth of the χ spectrum is controlled by the exponential factor $\exp(-\chi^2 a_1/4\beta)$. Thus the two apertures have the same $\Delta(\chi)$ bandwidth.

In the same vein, the temporal spectrum of the two apertures gives an idea of the required frequency bandwidths of the elements exciting the apertures. We define the temporal spectrum as

$$\phi_t(\rho,\ \omega) = \int_0^\infty \mathrm{d}\chi\chi J_0(\chi\rho)\phi(\chi,\omega). \tag{2.9}$$

The temporal spectrum of the Gaussian aperture is obtained by substituting Eq. (2.4) into Eq. (2.9) and integrating over χ, which is given explicitly as

$$\phi_t(\rho,\ \omega) = \frac{1}{4\beta}\int_0^\infty \mathrm{d}\chi\chi J_0(\chi\rho)\hat{\delta}_G[\omega - \omega_0(\chi);\ cT] \times \exp(-\chi^2 a_1/4\beta). \tag{2.10}$$

Equation (2.10) is plotted in Fig. 4, at $\rho = 0$. From the figure it is clear that the temporal spectrum closely resembles the spatial spectrum, thus showing the strong correlation between the temporal and spatial spectra. The temporal bandwidth is $f_{\max} = 19.1$ THz.

The substitution of Eq. (2.4) into Eq. (2.8) gives the periodic-aperture temporal spectrum:

$$\phi_t(\rho,\ \omega) = \frac{1}{4\beta}\int_0^\infty \mathrm{d}\chi\chi J_0(\chi\rho)\hat{\delta}_P[\omega - \omega_0(\chi);\ cT] \times \exp(-\chi^2 a_1/4\beta). \tag{2.11}$$

Numerical evaluation of Eq. (2.11) at $\rho = 0$ leads to a distribution that is indistinguishable from that of the Gaussian aperture. This result is expected, because for the Gaussian case we have an ω window centered at $\omega_0(\chi) = c[(\chi^2/4\beta) + \beta]$ and extending effectively from $\omega = [\omega_0(\chi) - 4/T]$ to $\omega = [\omega_0(\chi) + 4/T]$. As χ increases, the relative deviation of ω from its central value decreases. As an illustrative example, let us consider the deviation of ω from the central value at $\chi = 250\ \mathrm{m}^{-1}$. The central value $\omega_0(250)$ is 3.75×10^{12} rad/s, and the effective range of ω is $3.558 \times 10^{12} \leqslant \omega \leqslant 3.942 \times 10^{12}$ rad/s. Referring to Eq. (2.11), we notice that the central value of the periodic ω window is again at $\omega_0(\chi) = c[(\chi^2/4\beta) + \beta]$, which is the same as that of the Gaussian ω window. This ω window extends effectively from $\omega = [\omega_0(\chi) - 2.5\pi/T]$ to $\omega = [\omega_0(\chi) + 2.5\pi/T]$. At $\chi = 250\ \mathrm{m}^{-1}$ the central value of the ω window is the same as in the previous case. The range of ω is $3.373 \times 10^{12} \leqslant \omega \leqslant 4.127 \times 10^{12}$ rad/s. Hence it is clear that the width of the ω windows for both the Gaussian aperture and the periodic aperture are much smaller than the central value $\omega_0(\chi)$. For the integrations over χ in Eqs. (2.10) and (2.11), the narrow ω window sweeps the χ spectrum by varying $\omega_0(\chi)$ over an effective range having $0 < \chi < 4\beta/a_1$. Thus the bandwidths of the two ω windows are negligible in comparison with $\Delta(\omega) \cong \omega_0(\chi_{\max}) = 4c/a_1$. Consequently, the total bandwidth $\Delta(\omega)$ of the temporal spectrum of the periodic aperture is the same as that of the Gaussian aperture. In Section 3 it will be shown that in spite of this resemblance, the pulse radiated from the periodic aperture holds out for farther distances than the pulse launched by a Gaussian aperture.

3. FIELD PROPAGATING IN THE $Z>0$ HALF-SPACE

The excitation fields defined on the aperture are given in Eqs. (2.1) and (2.2). These fields can be expressed as a superposition of Bessel beams[1,2,18] at the plane $z = 0$; specifically,

$$\Psi_i(\rho,\ t) = \mathrm{Re}\left(\frac{1}{2\pi}\int_0^\infty \mathrm{d}\chi\chi J_0(\chi\rho)\int_0^\infty \mathrm{d}\omega\phi(\chi,\ \omega) \times \exp\{-i[\sqrt{(\omega/c)^2 - \chi^2}]z\}\exp(i\omega t)\right)_{z=0}. \tag{3.1}$$

The normal derivative of the field on the aperture is obtained by taking the derivative of the above expression with respect to z before we set $z = 0$. Furthermore, the quantity $\sqrt{(\omega/c)^2 - \chi^2}$ is restricted to positive values[1,2] to ensure the forward illumination of the aperture. The spectrum $\phi(\chi, \omega)$ is that given in Eqs. (2.4) or (2.5), depending on whether we are dealing with the Gaussian or the periodic aperture, respectively.

To calculate the outgoing field propagating into the $z > 0$ half-space, we apply Huygen's construction[19] to the initial excitation of the aperture. Accordingly, the field at a point $\mathbf{R}$ and time t inside a wave-front surface that has a zero field outside such a surface is given by the integration over the area of the aperture:

$$\Psi(\rho,\ z,\ t) = \frac{1}{4\pi}\int_0^{2\pi}\mathrm{d}\phi'\int_0^\infty \mathrm{d}\rho' \times \frac{\rho'}{R}\left[-\partial_{z'}\Psi(\rho',\ z' = 0,\ t') + \frac{z}{R^2}\Psi(\rho',\ z' = 0,\ t') + \frac{z}{Rc}\partial_{t'}\Psi(\rho',\ z' = 0,\ t')\right]_{t' = t - R/c}, \tag{3.2}$$

where $R = (\rho'^2 + \rho^2 - 2\rho'\rho\cos\phi' + z^2)^{1/2}$. The primed coordinates refer to source points on the aperture, and the unprimed ones refer to the observation points in the $z > 0$ half-space. The substitution of the initial field [Eq. (3.1)] into Eq. (3.2) yields[1–3]

$$\Psi(\rho, z, t) = \mathrm{Re}[\hat{\Psi}(\rho, z, t)], \tag{3.3a}$$

where

$$\hat{\Psi}(\rho, z, t) = \frac{1}{2\pi}\int_0^\infty d\chi\chi J_0(\chi\rho)\int_0^\infty d\omega\phi(\chi, \omega)\exp(i\omega t) \times \exp\{-i[\sqrt{(\omega/c)^2 - \chi^2}]z\}. \tag{3.3b}$$

The field launched from the Gaussian aperture into the $z > 0$ half-space is calculated by substituting Eq. (2.4) into Eq. (3.3) to produce

$$\Psi(\rho, z, t) = \frac{1}{8\pi\beta}\int_0^\infty d\chi\chi J_0(\chi\rho)\int_0^\infty d\omega \times \exp(-\chi^2 a_1/4\beta)\hat{\delta}_G[\omega - \omega_0(\chi); cT] \times \cos\{\omega t - [\sqrt{(\omega/c)^2 - \chi^2}]z\}. \tag{3.4}$$

The square root $\sqrt{(\omega/c)^2 - \chi^2}$ acquires only positive values[1,2] to ensure that all the field components are propagating away from the aperture. To study the decay pattern of the field given in Eq. (3.4) we shall concentrate on the centroid of the pulse at $z = ct$ for $t > 0$. The integration given in Eq. (3.4) is evaluated numerically. As z increases, the integrand becomes highly oscillatory. This leads to some difficulty in calculating the double integration (3.4). However, the numerical job can be reduced significantly if we utilize the fact that the ω window associated with the $\hat{\delta}_G$ function is relatively narrow. To further our understanding of Eq. (3.4), we refer to Fig. 2 (dotted curve), where it is clear that $\phi(0, \omega)$ represents a finite extension around a central value given by $\omega = c\beta$ and that all of its significant components lie in the range $(\beta - 4/cT)c \leq \omega \leq (\beta + 4/cT)c$. For values of χ other than zero the ω window is shifted by $\chi^2/4\beta$. Hence the integration over ω may be limited from $\omega = [\omega_0(\chi) - 4/T]$ to $\omega = [\omega_0(\chi) + 4/T]$, rather than extending over an infinite range.

The field radiated from the periodic aperture has an expression similar to that given by Eq. (3.4), with the Gaussian $\hat{\delta}_G$ function replaced by the periodic $\hat{\delta}_P$ function. One should note, however, that the extension of $\phi(0,\omega)$ is relatively larger than that of the Gaussian aperture, as clear from the solid curve in Fig. 2. Consequently, we choose the range of variation of ω to be between $\omega = [\omega_0(\chi) - 2.5\pi/T]$ and $\omega = [\omega_0(\chi) + 2.5\pi/T]$. The cosine term in Eq. (3.4) introduces oscillations inside the various ω windows. These oscillations depend on both χ and z. As χ increases, these oscillations decrease, but as z increases these oscillations increase. Thus the net area of the ω window decreases as z increases. Consequently, the field amplitude decays as it propagates away from the aperture.

Next we shall compare the characteristics of the decay of the pulse radiated from the Gaussian aperture with those of the decay of the pulse radiated from the periodic aperture. Figure 5 represents the decay of the centroid of the pulses radiated from both apertures at distances that are integer multiples of π/β. From the figure it is clear that near the aperture the Gaussian pulse holds out better than the periodic pulse. At larger distances, the periodic pulse not only overtakes the Gaussian pulse but also shows an obvious improvement in the decay rate with distance.

To further our understanding of the behavior of the pulses propagating away from the aperture, we analyze the spatial spectrum of each pulse at various distances. The spatial spectrum at any distance z is defined as

$$\phi_s(\chi, z, t) = \frac{1}{2\pi}\int_0^\infty d\omega\phi(\chi, \omega) \times \cos\{[\sqrt{(\omega/c)^2 - \chi^2}]z - \omega t\}. \tag{3.5}$$

The spatial spectrum of the Gaussian pulse at any distance z away from the aperture is obtained by substituting Eq. (2.3) into Eq. (3.5) to produce

$$\phi_s(\chi, z, t) = \frac{\exp(-\chi^2 a_1/4\beta)}{8\pi\beta}\int_0^\infty d\omega\hat{\delta}_G[\omega - \omega_0(\chi); cT] \times \cos\{[\sqrt{(\omega/c)^2 - \chi^2}]z - \omega t\}. \tag{3.6}$$

The integration given in Eq. (3.6) is evaluated numerically at different values of z, and the results are plotted in Fig. 6. From the figure it is clear that the low χ components decay rapidly with distance because of the high oscillations that are introduced into the ω windows sweeping the lower χ sections. We notice also that all spectral components decay with distance because the oscillations introduced for $z > 0$ always result in a loss of the net area of all the ω windows. This leads to the decrease of the amplitudes of the different sections of the spatial spectrum. One should emphasize, however, that the net losses in the ω windows centered around the lower χ sections are always greater than those for the higher ones.

Next we consider the spatial spectrum of the periodic pulse, which is given explicitly as

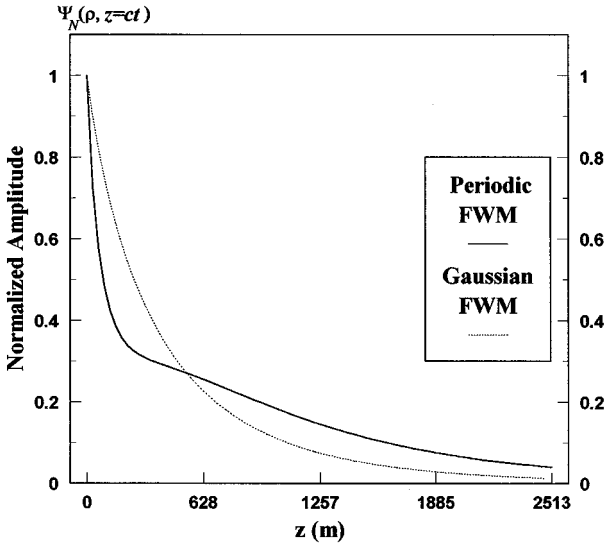

Fig. 5. Decay of the centroid of the periodic and the Gaussian pulses.

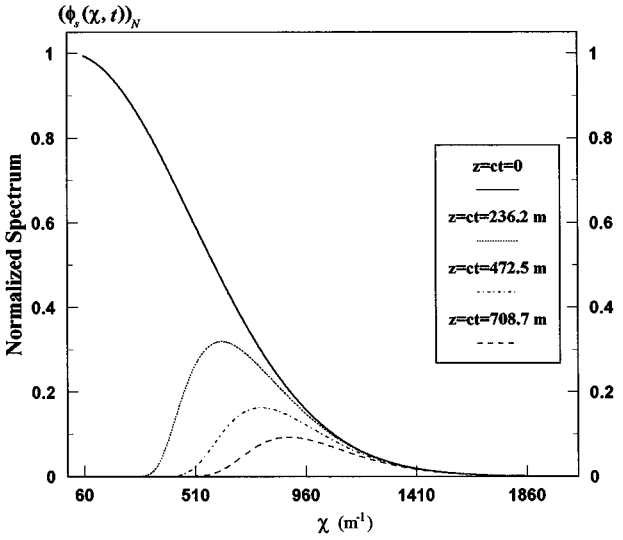

Fig. 6. Depletion of the spatial spectrum of the Gaussian FWM pulse with distance.

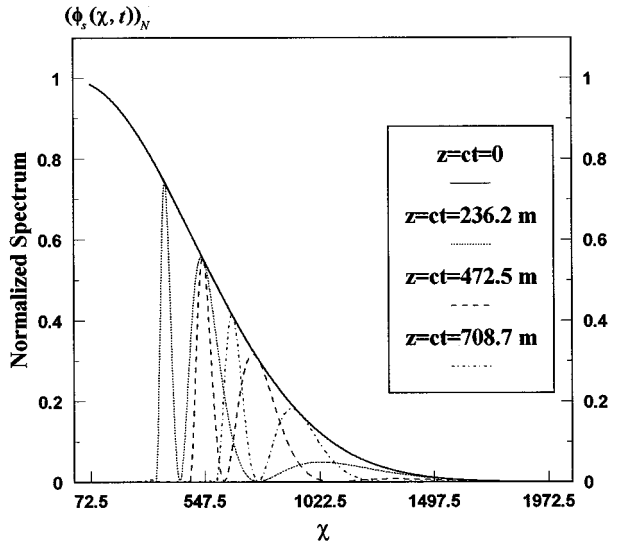

Fig. 7. Depletion of the spatial spectrum of the periodic FWM pulse with distance.

$$\phi_s(\chi, t) = \frac{\exp(-\chi^2 a_1/4\beta)}{8\pi\beta} \int_0^\infty d\omega \hat{\delta}_P[\omega - \omega_0(\chi); cT] \times \cos\{[\sqrt{(\omega/c)^2 - \chi^2}]z - \omega t\}. \quad (3.7)$$

The integration over ω is evaluated numerically for various distances z. Figure 7 represents the spectrum of Eq. (3.7). From the figure it is clear that the depletion of the spatial spectrum of the periodic pulse differs greatly from that of the Gaussian pulse. In this case the oscillations introduced into the spectrum result in conversion of the negative values of the spatial spectrum to positive ones and vice versa. This means that some components are added to the spectrum while others are subtracted. Such behavior results in an increase and a decrease, respectively, of the net area of the ω window at any constant χ section of the spatial spectrum as the distance is increased. Consequently, the amplitude of the pulse falls off quickly at shorter distances from the aperture. On the other hand, the narrow central lobe of the pulse's switching spectral window (see Fig. 2) slows down the deterioration of the χ spectral components by holding out against the introduced oscillations. This reduces the decay rate of the pulse as it propagates away from the aperture.

Furthermore, it is convenient to look at the decay of the central pulse with distance. The periodic and the Gaussian pulses are identical at $z = ct = 0$, and their power distribution is displayed in Fig. 8. From the figure it is clear that the minimum radius of the Gaussian pulse is $R_{\min} = 2.832$ mm. Near the aperture the periodic pulse

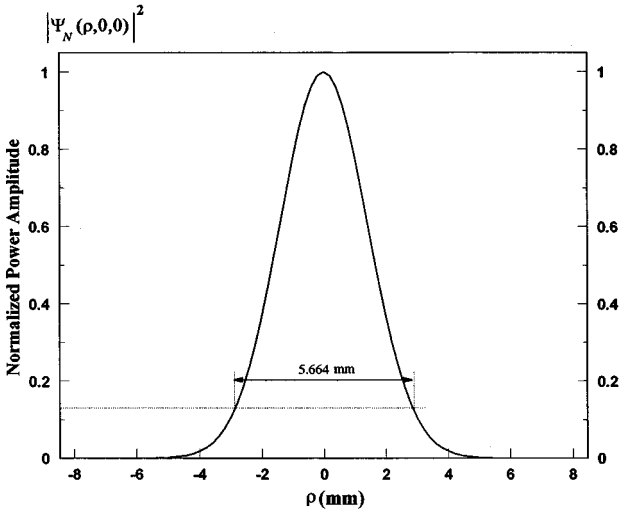

Fig. 8. Power amplitude of the FWM central pulse on the aperture at $z = ct = 0$.

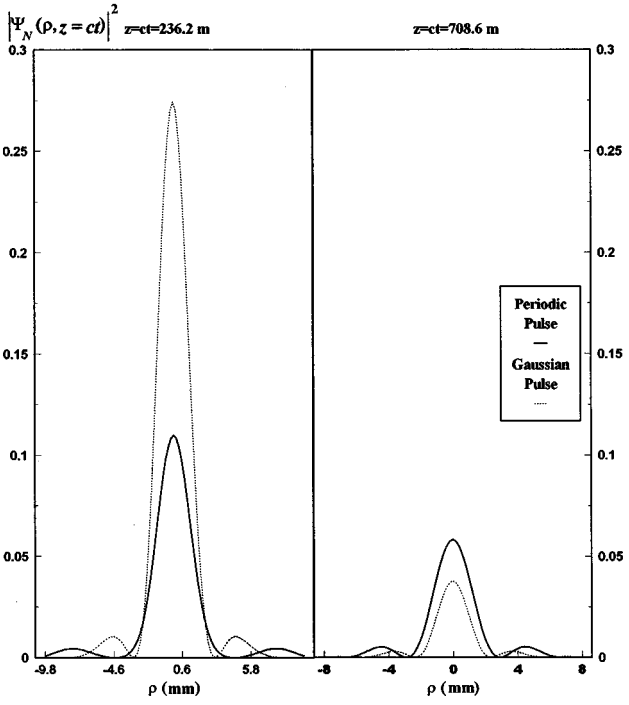

Fig. 9. Power amplitudes of the periodic and the Gaussian FWM central pulses at different distances from the aperture.

decays at a faster rate. The power content of the central Gaussian pulse is greater than that of the periodic pulse. This is clear from Fig. 9, which displays the power amplitude of both pulses at $z = ct = 236.2$ m. One should note that the displayed power amplitudes are normalized with respect to that of the central pulse at the aperture, i.e., at $z = ct = 0$. The power lost from the periodic pulse as it propagates to distances farther from the aperture is less than the power lost from the Gaussian pulse. Figure 9 also compares the two pulses at $z = ct = 708.6$ m. It is clear that at such a distance the power content of the periodic pulse is now greater than that of the Gaussian one. At large distances the power content of the central FWM pulse generated by a periodic excitation can be orders of magnitude greater than that of the Gaussian pulse. Thus the propagation characteristics of the two generated pulses have been shown to vary significantly, even though we have used two apertures that have the same maximum radius and the same temporal and spatial bandwidth but differ only in the form of the Fourier spectrum of the excitation time window.

4. CONCLUSION

In this paper we have studied the possibility of launching approximations to the FWM pulse from dynamic apertures. The type of aperture investigated varies its effective radius with time. We have studied two different windowing schemes to time limit the FWM excitation wave field. The first uses the Gaussian time window [Eq. (2.1)] and the other utilizes the periodic excitation given in Eq. (2.2). The causal fields generated by the apertures were calculated with Huygen's construction.[1,2,19] In the near-to-far-field range, the generated fields resemble the source-free FWM pulse[3,4] that has highly focused central Gaussians that hold out for extended ranges. We have demonstrated that the narrow central Gaussians generated by such apertures use the capabilities of their sources efficiently. This is the case because the energy of the illumination of a dynamic aperture[2] is always spread over its entire extension as it expands with time.

Apart from their excitation schemes, the two dynamic apertures that we have investigated are identical. They launch pulses having narrow Gaussian waists of equal extensions. Furthermore, they share the same spatial spectrum, and their temporal frequency bandwidths are equal. We have demonstrated that in spite of the similarity of the two sources, the generated localized pulses decay quite differently as they propagate away from their source plane. This is the case because the ranges of such highly focused pulses depend on the spatial–temporal distribution of the various elements constituting the sources. Thus one can control the range by temporally varying the sequence of the excitation of the various elements in a flat aperture. The coupling between the spatial and temporal frequency components ensues from the spectral $\hat{\delta}$ functions, which are directly related to the Fourier spectral content of the illumination sequence of the aperture. This explains how two identical sources can launch pulses that vary significantly as far as the decay of their amplitudes with distance is concerned. A detailed study of the depletion of the spectral components with distance, such as the one presented here, provides a decisive tool to design the decay pattern of a narrow pulse in the near-to-far field of its dynamic source. One should emphasize, however, that the case of the dynamic FWM aperture considered here is not the only possible way by which the excitation field of a narrow pulse is allowed to fill the extension of its source. Other possible schemes can be investigated simply by varying the transverse χ spectral content. This will change the manner by which the illuminating field fills up the aperture as the latter varies its size.

REFERENCES

1. A. M. Shaarawi, R. W. Ziolkowski, and I. M. Besieris, "On the evanescent fields and the causality of the focused wave modes," J. Math. Phys. **36**, 5565–5587 (1995).
2. A. M. Shaarawi, I. M. Besieris, R. W. Ziolkowski, and S. M. Sedky, "Generation of approximate focused-wave-mode pulses from wide-band dynamic Gaussian apertures," J. Opt. Soc. Am. A **12**, 1954–1964 (1995).
3. R. W. Ziolkowski, I. M. Besieris, and A. M. Shaarawi, "Aperture realizations of the exact solutions to homogeneous-wave equations," J. Opt. Soc. Am. A **10**, 75–87 (1993).
4. R. W. Ziolkowski, "Exact solutions of the wave equation with complex source locations," J. Math. Phys. **26**, 861–863 (1985).
5. A. M. Shaarawi, I. M. Besieris, and R. W. Ziolkowski, "Localized energy pulse trains launched from an open, semi-infinite, circular waveguide," J. Appl. Phys. **65**, 805–813 (1989).
6. P. Hillion, "Spinor focus wave modes," J. Math. Phys. **28**, 1743–1748 (1987).
7. A. M. Shaarawi, I. M. Besieris, and R. W. Ziolkowski, "A novel approach to the synthesis of nondispersive wave packet solutions to the Klein–Gorden and the Dirac equations," J. Math. Phys. **31**, 2511–2519 (1990).
8. A. M. Vengsarkar, I. M. Besieris, A. M. Shaarawi, and R. W. Ziolkowski, "Closed-form, localized wave solutions in optical fiber waveguides," J. Opt. Soc. Am. A **9**, 937–949 (1992).
9. M. K. Tippet and R. W. Ziolkowski, "A bidirectional wave transformation of the cold plasma equations," J. Math Phys. **32**, 488–492 (1991).
10. R. Donnelly and R. W. Ziolkowski, "A method of constructing solutions of homogeneous partial differential equations: localized waves," Proc. R. Soc. London Ser. A **437**, 673–692 (1992).
11. R. W. Ziolkowski, "Localized transmission of electromagnetic energy," Phys. Rev. A **39**, 2005–2033 (1989).
12. R. W. Ziolkowski, I. M. Besieris, and A. M. Shaarawi, "Localized wave representation of acoustic and electromagnetic radiation," Proc. IEEE **79**, 1371–1378 (1991).
13. R. W. Ziolkowski, "Properties of electromagnetic beams generated by ultra-wide bandwidth pulse-driven arrays," IEEE Trans. Antennas Propag. **40**, 888–905 (1992).
14. R. W. Ziolkowski, "Localized wave physics and engineering," Phys. Rev. A **44**, 3960–3984 (1991).
15. R. W. Ziolkowski and J. B. Judkins, "Propagation characteristics of ultrawide-bandwidth pulsed Gaussian beams," J. Opt. Soc. Am. A **9**, 2021–2030 (1992).
16. J. N. Brittingham, "Focus wave modes in homogeneous Maxwell's equations: transverse electric mode," J. Appl. Phys. **54**, 1179–1189 (1993).
17. I. M. Besieris, A. M. Shaarawi, and R. W. Ziolkowski, "A bidirectional traveling plane wave representation of exact solutions of the scalar wave equation," J. Math. Phys. **30**, 1254–1269 (1989).
18. J. Durnin, J. J. Miceli, Jr., and J. H. Eberly, "Diffraction-free beams," Phys. Rev. Lett. **58**, 1499–1501 (1987).
19. P. M. Morse and H. Feshbach, *Methods of Theoretical Physics* (McGraw-Hill, New York, 1953), Sec. 11.3.